JOURNAL OF MATERIALS SCIENCE 22 (1987) 4398–4402

Fractographic and acoustic emission of mullite–alumina–zirconia composites prepared by reaction sintering

C. BAUDIN*‡, F. CAMBIER§, L. DELAEY*
*Department of Metallurgy and Materials Engineering Katholieke Universiteit Leuven, Belgium and § Centre de Recherches de l'Industrie de la Céramique, Mons, Belgium

The fracture behaviour of a mullite–alumina–zirconia material prepared by reaction sintering has been studied by fractography and acoustic emission during indentation tests. The acoustic emission characteristics of the mullite composite are compared with those obtained from tetragonal zirconia polycrystal and aluminium oxide tested under the same conditions.

1. Introduction

Mullite–alumina–zirconia composites can be prepared by the reaction sintering of zircon–alumina mixed powders at lower temperatures and by using shorter firing times. The latter is possible by adding small quantities of oxides such as CaO, MgO and TiO_2 [1–3]. By a correct choice of the oxide quantities, the liquid phase should disappear during the subsequent heat treatment [4].

The fracture behaviour of these materials is not yet well understood. An attempt has been made to understand it by analysing the fracture surfaces [5], but no dynamic studies have been carried out. As a result of crack growth and plastic deformation, stress waves are emitted and detected as "acoustic emission" (AE). AE techniques are therefore ideal for analysing the deformation processes which take place during the fracture of ceramics. AE techniques have already been successfully applied to study microcracking as well as crack propagation in several structural ceramics as porcelain [6–8], aluminium oxide [9–14] and silicon carbide [13, 14] and also in glasses [12] and clay-based materials [15].

In the present work the fracture behaviour of a mullite–zirconia–alumina composite prepared from a mixture of zircon, alumina and magnesium oxide will be analysed and discussed. Details concerning the processing parameters and the main mechanical properties have been reported elsewhere [16]. The acoustic emission measured during indentation tests is compared with the AE emitted by aluminium oxide and tetragonal zirconia polycrystal (TZP). The fracture mode of the last two materials has already been analysed in detail in the literature [17, 18].

2. Experimental procedure

The fractography was performed by SEM on unetched as-fractured twin surfaces coated with evaporated gold. Indentation tests were made at different loads on polished surfaces of 3 mm thick specimens. These tests were carried out in an Instron machine with a hardness V136 indenter attached to one of the crossheads. The crosshead speed was 0.05 mm min^{-1} and the position of the crosshead was kept constant for 20 sec before unloading. The specimens were placed in a stainless steel cage using a grease as coupling agent. The AE transducer was placed on a rubber mount inside the cage to assure that no compression was exerted on it. The same grease ensured mechanical contact between the cage and the transducer.

The transducer was a PAC Type WD with a frequency band 100 to 900 kHz. The AE signals were amplified by an AET preamplifier with a gain of 60 dB and a frequency filter of bandwidth 100 to 1000 kHz. The signals were processed by an AET 5000 amplifier with an adjustable gain between 0 and 40 dB and a microprocessor. Real-time displays as well as post-processing facilities were available. The threshold voltage was fixed by setting the AE equal to zero for tests performed at loads for which no crack formation took place (loads $\leqslant$ 1 kg).

The median crack size, $2C$, arising from the indenter print corners, was determined as the average of the two radial cracks. The crack area was calculated as

$$\text{Area} = \frac{\overline{2C}^2}{2}\pi \qquad (1)$$

assuming that the crack has a half-penny geometry.

3. Results

3.1. Main fractographic features

The material consists of two well-differentiated microstructural areas: a mullite matrix in which zirconia and alumina particles are embedded and an amorphous silicate phase containing zirconia and several spinel particles as well as alumina submatrices. Alumina and zirconia particles form a link between both areas.

The principal fractographic features have been described elsewhere in more detail [5] and are summarized by the Figs 1 and 2. The fracture surface is

‡On leave from and now at Instituto de Ceramica y Vidrio Madrid, Spain.

0022–2461/87 $03.00 + .12

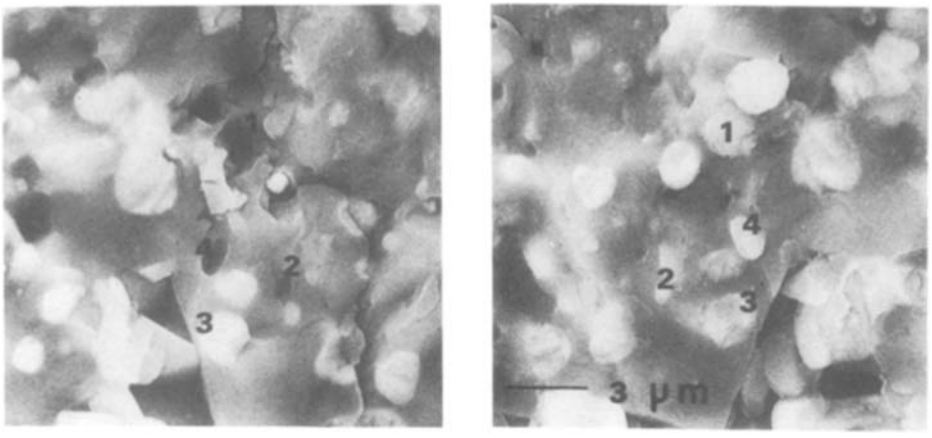

Figure 1 Pair of corresponding as-fractured surfaces showing the following main fractographic features: (1) uncrossed alumina particle embedded in the mullite matrix, (2) crossed intergranular zirconia particle, (3) crossed intergranular zirconia particle showing different cleavage planes, (4) uncrossed intergranular zirconia particle.

very irregular, the crack runs across the mullite matrix and changes its path depending on the different particles it encounters. The different features are marked with numbers on the figures. The alumina submatrices or single particles inside the mullite matrix ((1) in Fig. 1) present mainly an intergranular fracture mode. The crack runs across the alumina–alumina or alumina–mullite boundaries without being influenced by them. The zirconia particles present three kinds of fracture modes. Some of them show a single fracture plane ((2, 3) in Fig. 1); the largest and most irregularly shaped particles show several different oriented cleavage planes ((3) in Fig. 1) and the largest ($> 1.4\,\mu m$) round particles are surrounded by the crack ((4) in Fig. 1).

The principal features related to the amorphous phase are marked with letters. Flat fracture surfaces are not found in this phase; the crack path follows the boundaries between the amorphous phase and the mullite matrix ((a) in Fig. 2). The path of the crack is changed when the crack meets the zirconia and the alumina particles as also shown in Fig. 2. At (b) the irregular fracture of an alumina submatrix is shown, at (c) the alumina submatrix and zirconia particles are surrounded by the crack and (d) shows fractured zirconia particles. It should also be noticed that the crack path is not changed by the mullite–matrix grain boundaries and that the fracture mode of the matrix is mainly transgranular.

3.2. Acoustic emission measurements

The total number of AE events measured on Al_2O_3 is about one order of magnitude greater than registered on TZP and reaction-sintered mullite–alumina–zirconia.

Fig. 3 shows, as a function of the maximum applied load, the variation of the total number of AE events and the area of the crack surface calculated from Equation 1 for the three materials. For aluminium oxide, both quantities increase linearly with the maximum applied load. The AE activity emitted by TZP increases very fast for maximum loads higher than 400 N. The total number of AE events as well as the crack area of the mullite composite increases almost linearly with load, but the measurements show a larger scatter if compared with the results obtained from the other two materials.

Fig. 4 shows the shape of the AE measured as the number of ringdown counts against time for tests performed at two different maximum loads. The horizontal line in Fig. 4 indicates the time during which the crosshead of the Instron is kept fixed. For Al_2O_3 (Fig. 4c) the number of ringdown counts increases with time (i.e. load) and is maximum when the maximum load is reached and decreases while the Instron crosshead is kept fixed. There is no AE during unloading. For TZP (Fig. 4b) the AE increases with load and continues while the Instron crosshead is kept fixed. AE still continues during the unloading if the maximum load is high, i.e. ≈ 400 N. For the mullite composite (Fig. 4a) the AE emitted depends much upon the value of the maximum applied load. If the maximum load is low (e.g. 308 N), AE is measurable only during loading and unloading, whereas no AE is measured while the crosshead is kept fixed. For higher loads (e.g. 427 N), the major AE activity is measured while loading and also during the period that the crosshead is kept fixed. No AE is measured during unloading.

The distributions of AE events were measured as

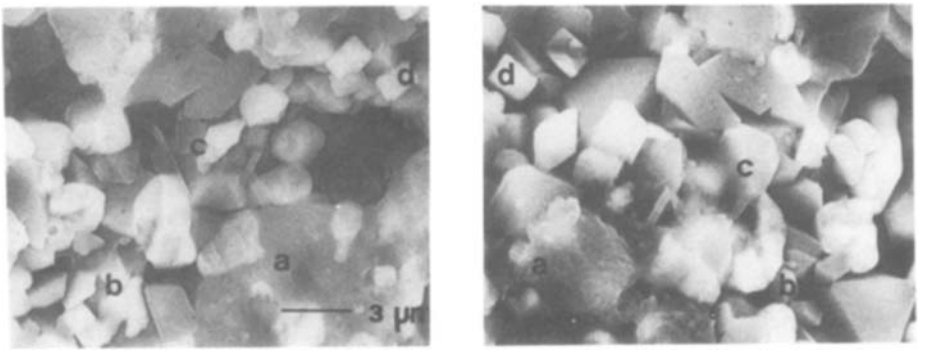

Figure 2 Pair of corresponding as-fractured surfaces showing the following main fractographic features: (a) glassy phase, (b) alumina submatrix showing alumina–alumina intergranular fracture, (c) crack surrounding the submatrices embedded in the amorphous phase, (d) zirconia particle showing a transgranular fracture mode.

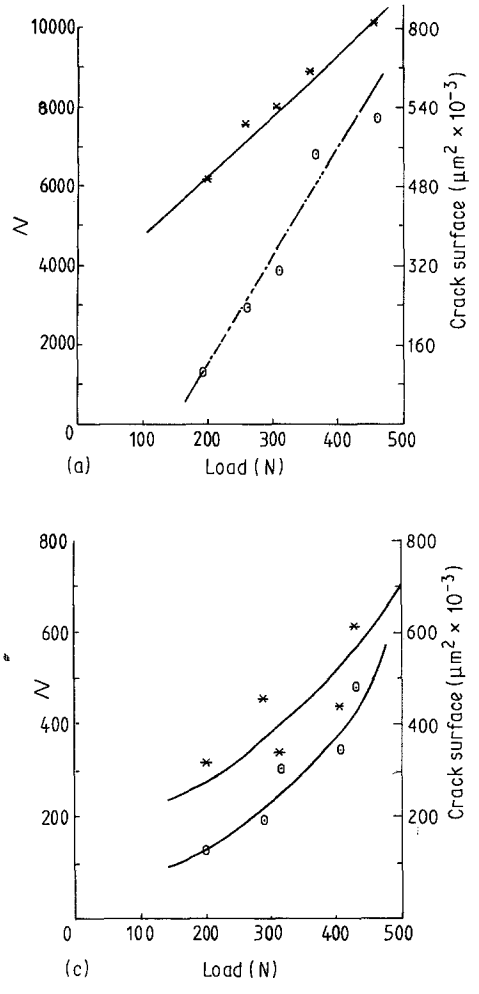

Figure 3 (*) Total number N of AE events and (⊙) crack surface against maximum load: (a) aluminium oxide, (b) tetragonal zirconia polycrystal, (c) mullite–alumina–zirconia composite.

a function of peak amplitude (in dB). Those corresponding to the tests of Fig. 4 are shown in Fig. 5. The b values corresponding to the fitting of the cumulative distribution plots [20] were also calculated as follows:

$$F(A) = (A/A_0)^{-b} \quad (2)$$

where A_0 is the lowest detectable amplitude. The calculation is made by fitting the plots of the logarithm of the cumulative distribution against the logarithm of the peak amplitude to a straight line, and the results are summarized in Table I.

The peak amplitude distribution does not change its shape when different loads are used for the mullite composite (Fig. 5a) and b values ranging from 0.13 to 0.16 are found for populations of events > 90%. The calculation [2] shows, upon increasing the load, a greater relative increase of the number of lower peak amplitude AE events. Fig. 5b shows for the TZP a clear shift towards the low peak amplitude values in the peak-amplitude distribution curve. Fig. 5c shows that, for aluminium oxide, the number of AE events with low amplitude (between 27 and 39 dB) increases with increasing load.

A good correlation to the power law [2] is found using populations ⩾90%, for loads under 300 N, $b \approx 0.09$ and the crossing with the Y axis ≈6.4. At

TABLE I Calculation of b values

Material	Maximum load (N)	Straight line		% total AE events	b	Crossing with Y axis	Correlation coefficient
		Min. PA*	Max. PA				
Al_2O_3	196	27	62	87	−0.09	6.32	0.997
	260	26	61	96	−0.09	6.46	0.994
	309	27	61	92	−0.09	6.47	0.997
	358	27	54	91	−0.11	7.15	0.989
		27	47	90	−0.09	6.54	0.994
		47	57	1 to 2	−0.13	8.21	0.985
	282	27	52	91	−0.11	7.16	0.988
		27	41	84	−0.08	6.27	0.9965
		41	52	6	−0.15	8.98	0.996
TZP	311	26	35	76.5	−0.10	4.72	0.994
	363	26	33	63.9	−0.07	3.55	0.978
	395	25	33	81	−0.09	4.30	0.976
	405	21	39	86	−0.05	3.24	0.998
	410	21	36	88	−0.07	4.12	0.996
Mullite–alumina–zirconia composite	204	27	41	99.7	−0.16	6.85	0.997
	284	27	38	88.4	−0.15	6.67	0.997
	308	26	41	99.1	−0.14	6.23	0.994
	407	20	39	97.8	−0.13	5.71	0.989
	427	26	38	90.1	−0.13	6.20	0.991

*Peak amplitude.

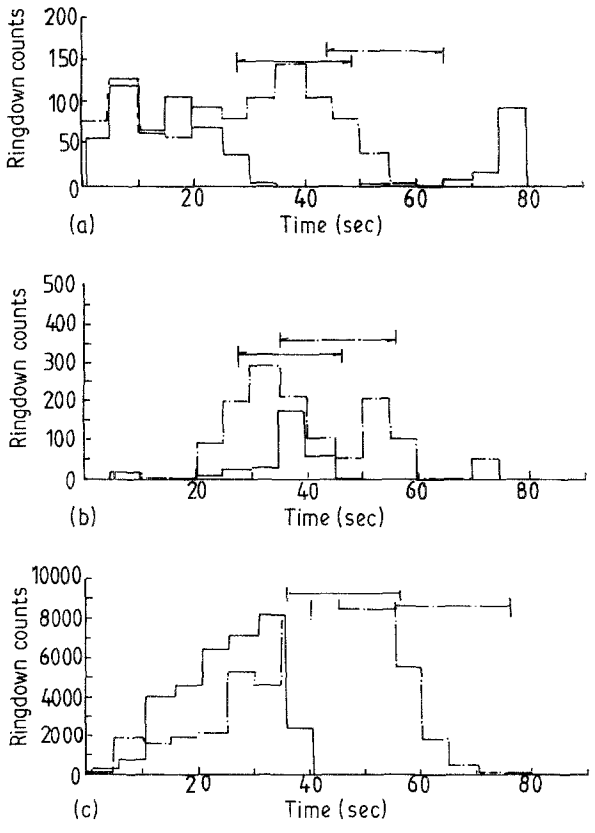

Figure 4 Total number of ringdown counts against time for tests performed using two different maximum loads. (a) Mullite–alumina–zirconia composite; maximum load (——) 300 N, (–·–·–·–) 427 N. (b) Tetragonal zirconia polycrystal; maximum load (——) 311 N, (–·–·–·–) 405 N. (c) Aluminium oxide; maximum load (——) 196 N, (–·–·–·–) 464 N.

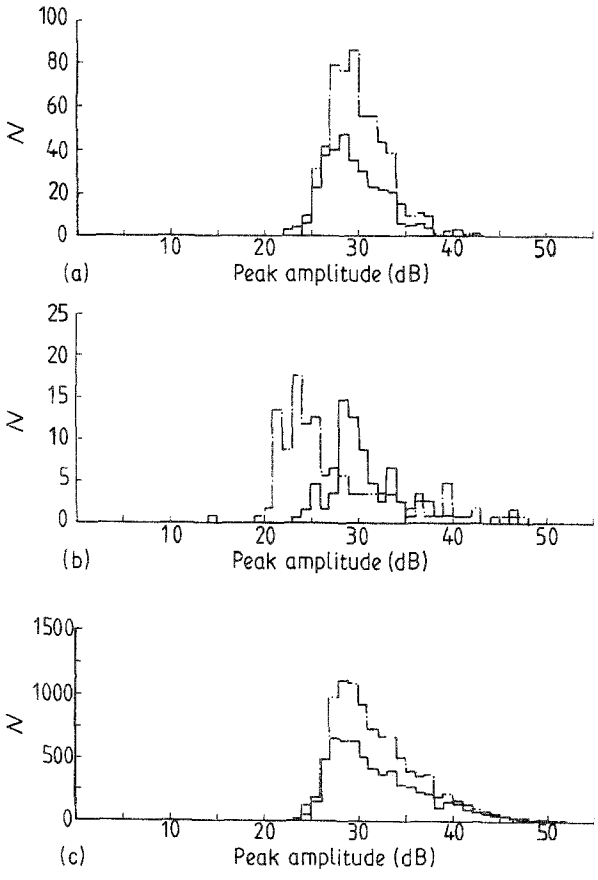

Figure 5 Peak amplitude distributions of number N of AE events for tests performed using two different maximum loads. (a) Mullite–alumina–zirconia composite; maximum load (——) 300 N, (–·–·–·–) 427 N. (b) Tetragonal zirconia polycrystal; maximum load (——) 311 N, (–·–·–·–) 405 N. (c) Aluminium oxide; maximum load (——) 196 N, (–·–·–·–) 464 N.

higher loads, the higher relative increase of the central part divides the cumulative distribution in two parts. One part corresponds with the low-amplitude events and one with the higher-amplitude events. The first part can be described with the same b value as above, whereas the second part (max. 6% of the events) can, for loads above 300 N, best be described by a b value of 0.11. Because the number of events to be fitted to the second part is rather small, only one mean fracture mechanism has to be considered.

4. Discussion

The total number of AE events increases with crack size as expected. The AE thus seems to provide us with good information concerning the damage which occurs in the samples during testing. In the case of TZP, the strong increase of this number for high loads could be related to the lower energy of those events, i.e. for the same amount of crack growth a larger number of low-energy events is needed.

In principle, the elastic–plastic indentation damage theory predicts that the median crack would attain its maximum growth during the loading half-cycle, whereas the radial crack is expected to continue its growth until unloading is complete [21]. The fact that no AE is measured during unloading could thus be in principle surprising. However, when experiments are performed in polycrystalline ceramics instead of in the "model" system soda–lime glass, the surface radial component becomes more dominant relative to the subsurface median in the earlier stages of loading as the ratio E/H increases [21, 22]. Experiments performed on silicon, where this ratio is 19, showed this enhancement of the radial crack growth during the loading half cycle if compared with soda–lime glass ($E/H \approx 13$). For the materials tested in the present work this relationship is about 20. It is thus very likely that the main growth of the crack takes place during loading.

Previous AE experiments performed on several different aluminas [11] also reveal such a behaviour. If only the relationship E/H were to be taken into account, the behaviour of the TZP as well as that of the mullite–alumina–zirconia composite would be the same. However, the AE detected in the tests performed on these materials reveals that the crack growth stops and does not continue until a larger amount of unloading takes place. This fact can now be related with the toughening mechanism which plays a role during the fracture of these two materials. The condition for equilibrium growth of the cracks is given by [21]

$$K = K_e + K_r = K_c \qquad (3)$$

where K_e is the elastic component and K_r the residual component, which are respectively compressive and tensile at the crack surface. The elastic component, being reversible, diminishes as the unloading takes place whereas the residual component, being irreversible, remains constant.

For toughened materials as TZP an R-curve behaviour (i.e. an increase of K_c as the crack size increases) has been found. Thus, when the crack has developed up to a certain size, it is necessary to increase further the stress concentration before obtaining further development of the crack.

For the TZP and the mullite–alumina–zirconia composite loaded until about 400 or 300 N, the growth of the crack stops and does not continue until K_e has diminished. For the TZP at lower loads (≈ 300 N), the decreasing of K_e is not enough to make the sum ($K_e + K_r$) equal to the new K_c, even when $K_e = 0$. In the mullite–alumina–zirconia composite at high loads (≈ 400 N), the sum $K_e + K_r$ equals K_c already at the onset of unloading. This is due to the relaxation of the load when the crosshead is kept fixed. The crack develops completely before unloading. This last fact reveals that the toughening mechanism in this material is weaker than in the TZP.

Crack growth proceeding in several different small jumps during unloading is clearly shown by the peak amplitude distribution of the AE events (Fig. 5b) obtained for the TZP at loads ≈ 400 N. The shape of this distribution shifts very strongly towards the low amplitude values.

The b value reflects how the total AE energy is divided. Thus, it is an absolute parameter that is used to compare several materials without being influenced by differences in damping of the original AE signal that take place in different materials. A low b value shows that the total AE energy is divided between a small number of events of high amplitude, whereas a high value reflects a division into a large number of low-energy events.

The lowest b values were obtained for the TZP samples. It seems that no subcritical events but only the main crack growth have been detected in the set of tests performed on this material. This growth is made up of several different jumps, which means that crack extension and arresting is taking place.

For the aluminium oxide this value was higher. The fracture mode which has already been determined for this material [17, 18] (i.e. microcracking around the particles followed by the coalescence of these microcracks) would be responsible for this.

The largest b value has been found for the mullite–alumina–zirconia composite, which means that the fracture energy is divided into a larger amount of different low-energy events. This fact can be correlated with the fractographic observations (Figs 1 and 2):

(i) low-energy events coming from the decohesion of the glassy phase (Fig. 2a);

(ii) higher-energy events ($K_{Ic} \approx 3\,MPa\,m^{1/2}$) coming from the fracture of the mullite–zirconia matrix (Fig. 1), and

(iii) slightly higher-energy events ($K_{Ic} \approx 3.7\,MPa\,m^{1/2}$) due to the cracking of the Al_2O_3 submatrices ((1) in Fig. 1, (b) in Fig. 2).

The branching of the main crack due to the existence of all those stress concentrators is then likely to be the toughening mechanism occurring in this material. For high loads (≈ 400 N) the damage to the material would be so large that the failure occurs by coalescence of microcracks. This fact is shown by the slight shift of the values of the Y axis crossing for high loads (see Table I).

Acknowledgements

The author would like to thank M. Wevers, D. Van Hulle, R. Van Daele and I. Verpoest of the K.U., Leuven, for valuable support in measuring the acoustic emission.

References

1. P. PENA, P. MIRANZO, J. S. MOYA and S. de AZA, *J. Mater. Sci.* **20** (1985) 2011.
2. P. MIRANZO, P. PENA, J. S. MOYA and S. de AZA, *ibid.* **20** (1985) 2702.
3. M. F. MELO, J. S. MOYA, P. PENA and S. de AZA, *ibid.* **20** (1985) 2711.
4. P. PENA, J. S. MOYA, S. de AZA, E. CARDINAL, F. CAMBIER, C. LEBLUD and M. R. ANSEAU, *J. Mater. Sci. Lett.* **2** (1983) 772.
5. C. BAUDIN, F. CAMBIER, and L. DELAEY, *J. Mater. Sci.* **21** (1986) 4024.
6. G. KIRCHOPP, W. PAMPE and H. A. BAHE, *ibid.* **17** (1982) 2809.
7. A. G. EVANS, S. M. WIEDHARN, M. LINZER and E. R. FULLER Jr, *Ceram. Bull.* **54** (6) (1975) 20.
8. A. G. EVANS and M. LINZER, *J. Amer. Ceram. Soc.* **56** (11) (1973) 575.
9. A. G. EVANS, M. LINZER and L. R. RUSSELL, *Mater. Sci. Eng.* **15** (1974) 253.
10. B. J. DALGHLEISH, P. L. PRATT, R. D. RAWLINGS and A. FAKHR, *ibid.* **45** (1980) 9.
11. R. D. RAWLINGS, *ibid.* **61** (1983) 62.
12. B. J. DAGHLEISH, A. FAKHR, P. L. PRATT and R. D. RAWLINGS, *J. Mater. Sci.* **14** (1979) 2605.
13. R. G. COOKE, in "Science of Ceramics 10", edited by H. Hausner (Deutsche Keramische Gesellschaft, 1980) p. 449.
14. H. H. HOELLER, T. POWERS, D. R. PETRAK and J. E. COUTTER, *SAMPE Q.* **16** (4) (1985) 44.
15. T. R. WILSHAW and R. ROTHWELL, *Nature Phys. Sci.* **229** (4) (1971) 156.
16. C. BAUDIN, A. LERICHE, F. CAMBIER and J. S. NOYA, *Silicates Industries* in press.
17. B. MUSSLER, M. V. SWAIN and N. CLAUSSEN, *J. Amer. Ceram. Soc.* **65** (11) (1982) 566.
18. A. G. EVANS, *ibid.* **68** (5/6) (1975) 239.
19. N. CLAUSSEN and M. RÜHLE, in "Science and Technology of Zirconia" (Advances in Ceramics Vol. 3), edited by A. H. Heuer and L. W. Hobbs (1981).
20. A. POLLOCK, *Non-destructive Testing* **6** (1973) 264.
21. B. R. LAWN, A. G. EVANS and D. B. MARSHALL, *J. Amer. Ceram. Soc.* **63** (9/10) (1980) 574.
22. A. G. EVANS and T. R. WILSHAW, *Acta Metall.*, **24** (1976) 939.

Received 9 February
and accepted 28 April 1987